ELSEVIER

NeuroImage

www.elsevier.com/locate/ynimg
NeuroImage 26 (2005) 1201 – 1210

Quantification of brain phosphodiesterase 4 in rat with (*R*)-[^{11}C]Rolipram-PET

Masahiro Fujita,[a,*] Sami S. Zoghbi,[a] Matthew S. Crescenzo,[a] Jinsoo Hong,[a] John L. Musachio,[a] Jian-Qiang Lu,[a] Jeih-San Liow,[a] Nicholas Seneca,[a] Dnyanesh N. Tipre,[a] Vanessa L. Cropley,[a] Masao Imaizumi,[a] Antony D. Gee,[b] Jurgen Seidel,[c] Michael V. Green,[c] Victor W. Pike,[a] and Robert B. Innis[a]

[a]*Molecular Imaging Branch, National Institute of Mental Health, Building 1, Room B3-10, 1 Center Drive, MSC-0135, Bethesda, MD 20892-0135, USA*
[b]*Translational Medicine and Technology, PET Division, GlaxoSmithKline, Addenbrooke's Hospital, Cambridge, UK*
[c]*National Institutes of Health, Bethesda, MD 20892, USA*

Received 26 January 2005; revised 11 March 2005; accepted 16 March 2005
Available online 29 April 2005

Objective: **Phosphodiesterase 4 (PDE4) catabolizes the second messenger 3′, 5′-cyclic adenosine monophosphate and may play a critical role in brain diseases. Our aim was to quantify PDE4 in rats with positron emission tomography (PET).** ***Methods:*** **High (n = 6) and low specific activity (SA) (n = 2) higher affinity ((*R*)-[^{11}C]rolipram) and high SA lower affinity ((*S*)-[^{11}C]rolipram) (n = 2) enantiomers were intravenously administered to Sprague–Dawley rats. Brain data were acquired using the ATLAS PET scanner and reconstructed using the 3D-ordered subset expectation maximization algorithm. Arterial samples were taken to measure unmetabolized [^{11}C]rolipram. Total distribution volumes (V'_T) were calculated using a 1-tissue compartment (1C) and an unconstrained 2-tissue compartment (2C) model.** ***Results:*** **High SA *R* experiments showed later and greater brain uptake, and slower washout than low SA *R* and *S* experiments. In all regions and in all experiments, the 2C model gave significantly better fitting than the 1C model. The poor fitting by the latter caused underestimation of V'_T by 19–31%. The 2C model identified V'_T reasonably well with coefficients of variation less than 10%. V'_T values by this model were 16.4–29.2 mL/cm^3 in high SA *R*, 2.9–3.5 in low SA *R*, and 3.1–3.7 in *S* experiments.** ***Conclusions:*** **Specific binding of (*R*)-[^{11}C]rolipram was accurately measured in living rats. In high SA *R* experiments, ~86% of V'_T was specific binding. Distribution and changes of PDE4 in animal models can now be studied by measuring V'_T of high SA (*R*)-[^{11}C]rolipram.**
Published by Elsevier Inc.

Keywords: Pharmacokinetics; Plasma metabolites; Cyclic AMP; Small animal PET; Compartment analysis

Introduction

3′, 5′-cyclic adenosine monophosphate (cAMP) is a prevalent second messenger that mediates signal transduction of several neurotransmitters including dopamine, epinephrine, histamine, and adenosine. cAMP is synthesized from adenosine 5′-triphosphate (ATP) by adenylyl cyclase and metabolized by cyclic nucleotide phosphodiesterases (PDEs). Thus, PDEs terminate the actions of the second messenger cAMP. At least 11 types of PDE exist in mammals, and PDE4 is selective to cAMP in the brain. PDE4 consists of four independently coded subtypes, PDE4A, B, C, and D (Houslay, 2001).

There is a large body of literature indicating that the cAMP pathway plays important roles in psychiatric illnesses, including mood disorders (Duman et al., 1997) and drug addiction (Nestler and Aghajanian, 1997). Among components of the cAMP pathway, PDE4 appears to be critical for antidepressant effects. Repeated antidepressant treatment increased PDE4 (Takahashi et al., 1999; Ye et al., 1997; Zhao et al., 2003), and an inhibitor of PDE4, 4-[3-(cyclopentoxyl)-4-methoxyphenyl]-2-pyrrolidone (rolipram), showed antidepressant effects both in animals (Mizokawa et al., 1988; Wachtel, 1983) and humans (Fleischhacker et al., 1992). However, adverse reactions such as emesis and sedation precluded rolipram from clinical applications. Rolipram is almost equipotent at all four PDE4 subtypes. Inhibitors selective to PDE subtypes may have therapeutic effects with minimal adverse reactions (O'Donnell and Zhang, 2004).

Rolipram has two enantiomers. The *R* enantiomer has 20 times greater affinity for PDE4 subtypes than the *S* enantiomer and racemic rolipram has a K_d of 1–2 nM (Schneider et al., 1986). In the brain, the density of the racemic rolipram binding sites is high (20 nM) (Schneider et al., 1986) compared to other proteins that have been successfully imaged in vivo, and the lipophilicity of rolipram (Log P = 2.9) appears to be appropriate for brain

* Corresponding author. Fax: +1 301 480 3610.
E-mail address: FujitaM@intra.nimh.nih.gov (M. Fujita).
Available online on ScienceDirect (www.sciencedirect.com).

1053-8119/$ - see front matter. Published by Elsevier Inc.
doi:10.1016/j.neuroimage.2005.03.017

imaging (Waterhouse, 2003). Considering the importance of PDE4 in diseases, high density of PDE4, and chemical characteristics of (*R*)-rolipram, this compound may be quite promising as a brain imaging agent. In fact, following initial rodent studies (Lourenco et al., 1999, 2001), (*R*)-[^{11}C]rolipram has been successfully applied in non-human primates (Tsukada et al., 2001) and humans (DaSilva et al., 2002; Matthews et al., 2003). PDE4 is activated by phosphorylation with protein kinase A (Conti et al., 1995), and a study using recombinant DNAs has indicated that phosphorylation of PDE4 affects the binding affinity of rolipram (Hoffmann et al., 1998). Therefore, in addition to measuring binding density and affinity, (*R*)-[^{11}C]rolipram-positron emission tomography (PET) imaging may provide information on the phosphorylation state of PDE4.

Many studies have been performed on rodents to assess pathologic changes of the cAMP pathway. Recent development of small animal PET scanners has opened possibilities of exploring such changes in living animals. Compared to larger animals, it is easier to prepare disease models and administer drugs to rodents. However, it may be difficult to perform accurate PET quantification using small animals because of the small body size. Physiological conditions can change easily and it is difficult to obtain large volumes of blood samples for input function measurement. Prior studies of [^{11}C]rolipram in humans and non-human primates were not quantitative and did not distinguish changes in delivery of radioligand from changes in density of PDE4. In this study, we measured distribution volume of high specific activity (SA) (*R*), low SA (*R*), and high SA (*S*)-[^{11}C]rolipram in rat brain by applying compartmental nonlinear least squares analysis. Because rolipram binding sites are widely distributed in the rat brain (Kaulen et al., 1989; Perez-Torres et al., 2000), no reference tissue was available and an arterial input function was required for the quantification.

Materials and methods

Radioligand preparation

(*R*) and (*S*)-[^{11}C]rolipram were synthesized by ^{11}C-methylation of (*R*) and (*S*)-*desmethyl*-rolipram, respectively. Specifically, [^{11}C]iodomethane was prepared via a GE Microlab (Milwaukee, WI, USA) and swept with helium carrier gas (ca. 12 mL/min) into a commercial radiomethylation loop apparatus (AutoLoopTM, Bioscan, Washington DC, USA). [^{11}C]Iodomethane was reacted at room temperature for 3 min with phenolic precursor (0.3 mg) dissolved in *N*,*N*-dimethylformamide (0.08 mL) and a solution of tetrabutylammonium hydroxide (0.17 M) in methanol (3 μL). HPLC on an Ultrasphere C-18 column (10 × 250 mm; Beckman C-18) eluted with acetonitrile-0.1 M ammonium formate (40: 60 v/v) at 6 mL/min was used to purify the radioligand (R_t = 6.5 min). Rotary evaporation of the collected fraction to dryness at 80°C under vacuum followed by formulation of the residue in 10% (v/v) ethanol in normal saline afforded either the *R* or *S* radioligand in high radiochemical purity (>95%). (*R*) and (*S*)-[^{11}C]rolipram were finally dissolved in normal saline for intravenous injection.

Animals

All animal experiments were performed in accordance with the National Institutes of Health Guide for Care and Use of Laboratory Animals and were approved by the National Institute of Mental Health Animal Care and Use Committee. Male Sprague–Dawley rats were obtained from Taconic Farms (Germantown, NY, USA). Before use for experiments, animals were housed in a temperature- (22–24°C) and light- (on 6:00 AM–6:00 PM) controlled room and were allowed free access to food pellets and water.

PET

Ten male Sprague–Dawley rats (314 ± 35 g, with these and subsequent data expressed as mean ± SD) were used in PET studies with arterial blood sampling and kinetic modeling. Under 1–1.5% isoflurane anesthesia, an Intramedic PE-10 polyethylene catheter (Aster Industries, Harmony, PA, USA) was inserted into a femoral artery for arterial blood sampling, and another catheter of the same type was inserted into a penile vein for injection of [^{11}C]rolipram. For three of the 10 animals, anesthesia was induced by co-injections of ketamine and xylazine (50–100 and 5–10 mg/kg i.p. per dose, respectively) and then switched to isoflurane anesthesia. The minimal interval between the last ketamine and xylazine administration and the injection of [^{11}C]rolipram was 129 min. To prevent movement, the head and the body were restrained with tapes to the camera bed.

High SA (*R*), low SA (*R*), and high SA (*S*)-[^{11}C]Rolipram were injected into six, two and two rats, respectively. SA was 71 ± 10, 0.19 or 0.38, and 55 or 71 GBq/μmol in high SA *R*, low SA *R*, and high SA *S* experiments, respectively. In the low SA experiments, racemic rolipram was mixed with (*R*)-[^{11}C]rolipram; the SA shown above is based on molar amount of (*R*)-rolipram and the mass dose was 0.28 and 0.63 mg/kg. The radioligands were dissolved in saline (1.3 ± 0.5 mL) and infused into a penile vein using a syringe pump (Harvard PhD 2000, Harvard Apparatus, Holliston, MA, USA). The radioligands were infused over 6 min because nearly 1 min was necessary to obtain each arterial blood sample (150 μL) for radioactive metabolite analysis at initial time points; rodents generally metabolize xenobiotics quickly and several samples at different times were required. If radioligand had been injected over 30 to 60 s, changes of the input function would have not been caught by the slow blood sampling. After finishing the 6-min infusion of the radioligand, plasma levels of rolipram may decrease quickly and such changes may not be detected by blood sampling every 1 min. Therefore, a higher infusion rate was applied from 0 to 3 min and then a lower rate was applied from 3 to 6 min. The ratio of these two infusion rates was 3 to 1. PET data were acquired by the Advanced Technology Laboratory Animal Scanner (ATLAS) equipped with lutetium gadolinium oxyorthosilicate doped with cerium (LGSO)/gadolinium oxyorthosilicate doped with cerium (GSO) phoswich detector modules providing 6.0 cm transverse filed-of-view (FOV) and 2.0 cm axial FOV (Seidel et al., 2003). PET data were acquired for 80 min in frames of 6 × 20 s, 5 × 1 min, 4 × 2 min, 3 × 5 min, 3 × 10 min and 1 × 20 min. Arterial blood samples were taken into heparin-coated tubes (Anticoagulant-coated microcentrifuge tube, Thomas Scientific, Swedesboro, NJ, USA) eight times between 0 and 10 min and at 20, 40, and 60 min (i.e., a total 11 time points). The sampling volume was 150 μL for the initial eight samples and 500 μL for the last three samples.

Throughout PET scanning, body temperature was maintained by a heating pad and monitored by a rectal temperature probe. Average deviation of body temperature from 37.0°C during the ten scans was 0.3 ± 0.2°C. Heart rate was also monitored with an ECG

(Biopac Systems, Inc., Goleta, CA, USA); and the maximum change of heart rate within each scan was 15 ± 8%.

Measurement of plasma [^{11}C]rolipram levels

Plasma samples (50–80 μL) were mixed with acetonitrile (300 μL) containing reference rolipram. Distilled water (100 μL) was then added and mixed well. This mixture was counted in a calibrated gamma counter for measurement of total concentration of radioactivity. The deproteinized plasma samples were then centrifuged at 9400 × *g* for 4 min to remove the denatured proteins. The supernatant was then analyzed directly by reversed phase high-performance liquid chromatography (HPLC) on Novapak C18 (Waters Corp., Milford, MA, USA) within a radial compression module RCM-100, eluted with MeOH: H_2O: Et_3N (80: 20: 0.1 by vol.) at 1.5 mL/min. The precipitate was counted in the gamma counter and the percent recovery of radioactivity in the supernatant was calculated. All radioactivity measurements were decay-corrected to the time of dose administration.

Image analysis

PET data were reconstructed with 3D exact positioning ordered subset expectation maximization algorithm with sixteen subsets and three iterations, achieving a 1.7-mm full width half maximum at the center (Johnson et al., 2002; Liow et al., 2003). Movement of head during scanning sessions was visually inspected. In two experiments in which movement was detected, images were coregistered using the rigid body model of Oxford Centre for Functional Magnetic Resonance Imaging of the Brain (FMRIB)'s Linear Image Registration Tool (FLIRT). FLIRT was implemented in MEDx 3.42 (Medical Numerics, Inc., Sterling, VA, USA).

To minimize inconsistencies in volume of interest (VOI) placement among animals, all frames of PET images were transformed into a standard space (Schweinhardt et al., 2003). First, a common template image of the three experimental paradigms, that is, high SA *R*, low SA *R*, and high SA *S* experiments, was created by the following procedures. Images of 0–7 min in each experiment of the three paradigms were integrated. The period of the first 7 min was used because regional differences in activities among the three paradigms were minimal (see below). Then, the integrated images of all experiments were manually realigned to the same orientation and an average image was created from all realigned images. With Statistical Parametric Mapping (SPM) 2 (Wellcome Department of Cognitive Neurology, London, UK; http://www.fil.ion.ucl.ac.uk/spm), this average image was spatially normalized to the standard space defined by the smoothed T2 weighted MRI template (Schweinhardt et al., 2003). Then, this spatially normalized PET image was used as a common template for all three paradigms to which images of each experiment were normalized using SPM 2. For each experiment, an integrated image from the first 7 min was spatially normalized to the rolipram template. Using transformation parameters obtained in this spatial normalization, images of all frames were spatially normalized to the standard space.

On a non-smoothed T2-weighted template in the standard space, VOIs were drawn on caudate putamen (volume: 29 mm^3), thalamus (31 mm^3), hypothalamus (19 mm^3), hippocampus (33 mm^3), frontal (14 mm^3), parietal (80 mm^3), and temporal (35 mm^3) cortices and midbrain (29 mm^3). VOIs were not placed on occipital cortex and cerebellum because part of these regions was close to the border or out of the field of view (FOV). A VOI was also drawn on the entire brain within the FOV.

Binding of radioligands to plasma proteins

Because of the short half life of carbon-11 ($t_{1/2}$ = 20.4 min), it was impossible to measure radioactive metabolites in plasma and the binding of radioligand to plasma proteins in the same experiment. Therefore, binding to plasma proteins was measured in separate experiments without PET imaging. After ketamine and xylazine administration (100 and 10 mg/kg i.p., respectively), blood (3 mL) was drawn from the heart of three male Sprague–Dawley rats. Blood samples from one and two rats were used to measure protein binding of *R* and *S* enantiomers, respectively. Plasma protein binding was measured by ultrafiltration through Centrifree membrane filters (Amicon Division, W.R. Grace and Co., Danvers, MA, USA) (Gandelman et al., 1994).

Derivation of rate constants and distribution volumes

Plasma (*R*) or (*S*)-[^{11}C]rolipram were used as the input function for compartmental nonlinear least squares analyses. For the time points before the peak of plasma [^{11}C]rolipram activity, measured values were used; after the peak, values were estimated with bi-exponential fitting. Each model configuration was implemented to account for the time shift between the plasma input function measured from the femoral artery and the actual arterial input to the brain. In each model and in each study, the time shift was estimated first by fitting the entire brain data. Then, this estimated shift was used to fit all brain data from the same study using the same model. Brain data were weighted based on noise equivalent count.

One-tissue and unconstrained two-tissue compartment models were applied. Rate constants (K_1, k_2, k_2', k_3, and k_4) were defined as described previously (Laruelle et al., 1994). In the one-compartment model,

$$V_T = \frac{K_1}{k_2' f_1} \tag{1}$$

where V_T is the distribution volume for the single tissue compartment. In the two-compartment model, V_T is described separately by the distribution volumes in nondisplaceable (V_N) and specific binding compartments (V_S).

$$V_N = \frac{K_1}{k_2 f_1} \tag{2}$$

$$V_S = \frac{K_1 k_3}{k_2 k_4 f_1} = \frac{B'_{max}}{K_d} \tag{3}$$

$$V_T = \frac{K_1 (1 + k_3/k_4)}{k_2 f_1} \tag{4}$$

where B'_{max} is unoccupied binding site density. Under tracer conditions, $B'_{max} = B_{max}$. In these two models, although the definition of K_1 is the same, that of k_2 and k_2' is different. That is, k_2 is transfer rate to the vascular compartment from the nondisplaceable compartment in the two-compartment model, and k_2' refers to the transfer from the total tissue compartment (Laruelle et al., 1994).

V_i' is defined as

$$V_i' = f_1 V_i \tag{5}$$

These definitions indicate that V_i values are expressed relative to the free fraction of radioligand in plasma and that V_T' values are expressed relative to the total (free plus protein-bound) concentration of radioligand in plasma. Throughout the text, brain and blood volumes are shown as cm^3 and mL, respectively, to indicate the source of the data.

Non-linear least-squares analysis was performed on the VOI-generated time-activity data using PMOD 2.55 (Burger et al., 1998). Parameters were estimated using the Marquardt algorithm (Bevington and Robinson, 2003) with constraints restricting parameters to positive values.

Ex vivo experiments

To further define the distribution of in vivo rolipram binding, an ex vivo autoradiography experiment was performed using a 165-g male Sprague–Dawley rat. Under isoflurane anesthesia, racemic [^{3}H]rolipram (3.1 MBq, SA = 3.0 GBq/μmol) in ethanol (Amersham Biosciences Inc, Piscataway, NJ, USA) was injected at a constant rate (35 μL/min) over 12 min into a femoral artery. The rat was decapitated at 40 min after starting rolipram injection. The brain was immediately frozen in dry ice and stored at −70°C until sectioning. Using a cryostat, the brain was cut to 20 μm coronal sections and thaw-mounted onto poly-L-lysine coated glass slides (Sigma-Aldrich, Natick, MA, USA). The slides were exposed to a ^{3}H imaging plate (TR2025, Fujifilm, Stamford, CT, USA) for 26 days. A set of ^{3}H standards (Amersham Biosciences Inc, Piscataway, NJ, USA) was exposed with the slides to calibrate radioactivity to Bq/mg tissue equivalent. The density of ^{3}H binding sites in brain regions was analyzed using an image analysis program (Image Gauge, ver. 2.3, Fujifilm, Stamford, CT, USA).

To study if radioactive metabolites enter the brain, (*R*)-[^{11}C]rolipram (61 MBq; SA = 142 GBq/μmol) was intravenously injected over 1 min to a male Sprague–Dawley rat (300 g) under ketamine and xylazine anesthesia (50 and 5 mg/kg i.p., respectively). At 30 min after the injection, the rat was decapitated, the whole brain was sampled, and radioactive compounds were analyzed with HPLC.

Statistical analysis

The standard errors of nonlinear least-squares estimation for rate constants were given by the diagonal of the covariance matrix (Carson, 1986) and expressed as a percentage of the rate constants (coefficient of variation, %COV). In addition, %COV of V_T' was calculated from the covariance matrix using the generalized form of error propagation equation (Bevington and Robinson, 2003) where correlations among parameters (K_1, k_2 (k_2'), k_3, and k_4) were taken into account. The accuracy of distribution volume estimation was evaluated by %COV, bias of results, and variability among experiments.

Goodness-of-fit by nonlinear least-squares analysis was evaluated using the model selection criterion (MSC), which is a modification of the Akaike information criterion (AIC) (Akaike, 1974). MSC was proposed by Micromath Scientific Software (Salt Lake City, Utah, USA) and implemented in their program, 'Scientist'. MSC is adjusted by the number and the levels of data points so that comparisons can be made among fittings for different studies and regions. Among fittings for the same data set, MSC and AIC give the same rank order although the former gives greater values for better fitting. We used MSC to evaluate goodness-of-fit in our previous study (Fujita et al., 1999). Goodness-of-fit by one- and two-compartment models was compared with *F* statistics (Hawkins et al., 1986).

Correlations were tested by simple correlation analysis and the determination of Pearson's product-moment correlation coefficient (*r*). Comparison between the two compartmental models was performed by paired *t* test. Comparisons among high SA *R*, low SA *R*, and high SA *S* experiments were performed with repeated measures multivariate analysis of variance (MANOVA) with Tukey's honestly significant difference test. A value of $P < 0.05$ was considered as significant. SPSS 12.0 (SPSS Inc. Chicago, IL, USA) was used for statistical analyses.

Results

Kinetics of PET brain data

Compared to low SA *R* and high SA *S* experiments, high SA *R* experiments showed typical characteristics of specific binding, with greater peak activity, slower washout from the brain, and heterogeneous distribution. Fig. 1 shows dynamic changes in brain activities during PET studies with high SA (72 GBq/μmol) (*R*), low SA (0.38) (*R*), and high SA (55) (*S*)-[^{11}C]rolipram experiments. To compare results among different experiments, activity is normalized to injection dose and body weight by use of the standard uptake value, SUV% [SUV% = (% injection dose/cm^3 brain) × body weight (g)]. A SUV of 100 % is equivalent to a uniform distribution of injected activity in the whole body. Compared to low SA *R* and high SA *S* experiments, high SA *R* experiments showed greater activity at all time points. Although activities in the brain were apparently greater than those in extra-brain tissues at all three time points in the high SA *R* study, activities in the brain were greater than those in extra-brain tissues only at 0–11 min in low SA *R* and high SA *S* experiments. Among the three types of experiments, only the high SA *R* experiments showed regional differences in activities and kinetics. In those experiments, compared to cerebral cortices, the thalamus initially showed greater and then showed similar activity. Because data in cerebral cortices were similar, those in parietal cortex are described below as a representative of cerebral cortices.

High SA *R* experiments showed average peak uptake at 9.6, 6.8, 5.8, 7.8, 9.3, and 5.7 min in caudate putamen, thalamus, hypothalamus, hippocampus, parietal cortex, and midbrain, respectively. At the end of the experiments, activities in these regions were 51, 44, 40, 52, 59, and 38% of the peak, respectively. In the same regions, low SA *R*-experiments showed peaks at 4.0–5.0 min, and at the end of the experiments, activities were 18–35% of the peaks. High SA *S* experiments showed peaks at 3.5–4.0 min, and at the end of the experiments, activities were 14–21% of the peaks.

Distribution of rolipram binding in vivo

As described above, only high SA *R* experiments showed regional differences in activity. Regional distribution was studied in two ways, firstly, brain regions were identified by performing spatial normalization to published standard space. Secondly, to confirm distribution with greater spatial resolution, an ex vivo

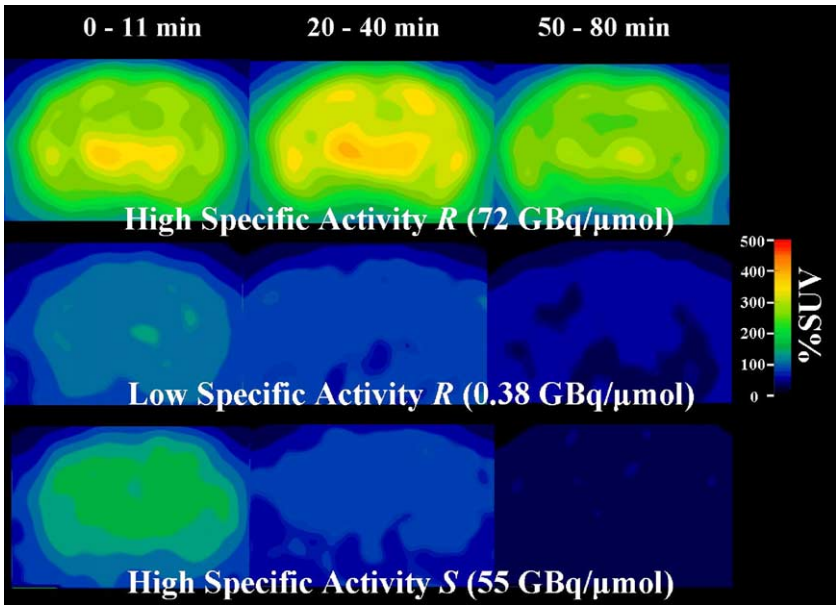

Fig. 1. Coronal slices in the same location of high SA (*R*), low SA (*R*), and high SA (*S*)-[^{11}C]rolipram PET experiments at 0–11, 20–40, and 50–80 min. All images are spatially normalized to the standard space (Schweinhardt et al., 2003). Integrated images during the three time periods are shown. Compared to low SA *R* and high SA *S* experiments, the high SA *R* experiments showed greater activity, slower washout, and more heterogeneous distribution of activity.

autoradiography experiment was performed (Fig. 2). PET images of high SA *R* experiments showed fairly uniform distribution with greater activity in the thalamus and smaller activity in hypothalamus and midbrain. On PET images, the distribution of activity appeared uniform in thalamus and hypothalamus, and differential distribution among nuclei was not clear. Ex vivo autoradiography showed distribution similar to that of PET. However, autoradiography showed more heterogeneous distribution within thalamus than did PET (Table 1). Rostral thalamic nuclei showed uniform and high binding with 38 Bq/mg tissue. On caudal side, posterior and parafascicular nuclei showed a low level binding of 21 while the binding in lateral and medial geniculate and ventroposterior nuclei was apparently greater with 35, 33, and 36 Bq/mg tissue, respectively. Cerebral cortices showed uniform distribution, and the activity was low in hypothalamus and midbrain. Because a significant portion of the cerebellum was out of FOV, there were errors in the spatial normalization in areas close to the caudal border of FOV as seen on the right PET image in Fig. 2.

The HPLC analysis on the whole brain obtained at 30 min after a bolus injection of (*R*)-[^{11}C]rolipram showed that 97.3% of the radioactive compounds in the brain was (*R*)-[^{11}C]rolipram.

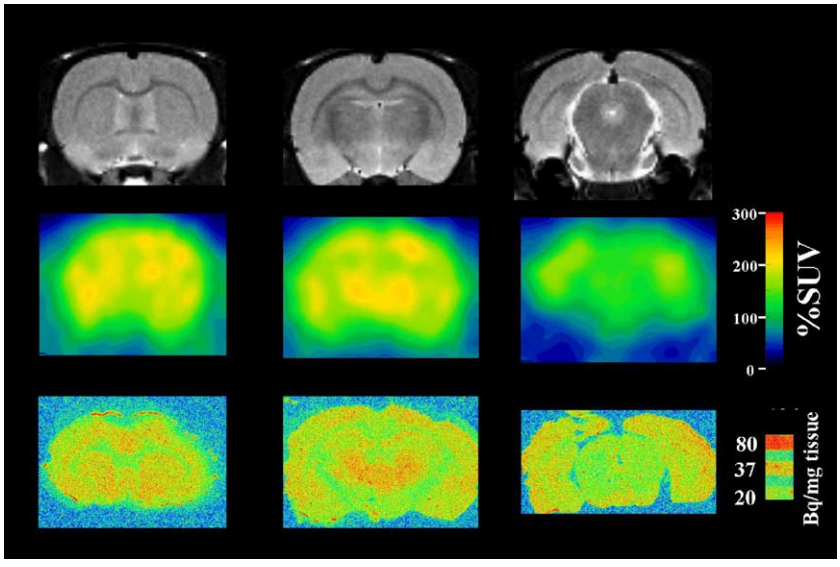

Fig. 2. Distribution of rolipram binding in vivo. Top, middle, and bottom rows show T2-weighted MR images, integrated images from all time points of a high SA (*R*)-[^{11}C]rolipram PET experiment, and ex vivo autoradiograms using racemic [^{3}H]rolipram, respectively. MR and PET images are in the standard space (Schweinhardt et al., 2003). In the PET images, thalamus showed greatest activity followed by caudate putamen and cerebral cortices. Hypothalamus and midbrain showed low activity. The distribution of rolipram binding in the ex vivo autoradiography was similar to that of the PET experiments. Compared to cerebral cortices (31 Bq/mg tissue), thalamus showed greater (38), hypothalamus (22) and midbrain (19) showed lower activities.

Table 1
Distribution of activity in ex vivo autoradiography

		Activity (Bq/mg tissue)
Cerebral cortices	Frontal	33.0
	Parietal	29.6
	Temporal	31.3
	Occipital	33.5
Thalamus	Nuclei not specified below	37.7
	Lateral geniculate	35.0
	Medial geniculate	33.3
	Ventroposterior	35.8
	Posterior and parafascicular	20.6
Hypothalamus		22.3
Caudate putamen		31.2
Hippocampus		27.0
Midbrain		19.0

Plasma data

In all experiments, [^{11}C]rolipram was metabolized and quickly cleared from plasma (Fig. 3). Bi-exponential fitting for [^{11}C]rolipram levels showed half-lives of 2.1 and 24 min with a 5:1 ratio of the height of the peaks for high SA *R*. Low SA *R* decreased with half lives of 2.2 and 22 min with a ratio of 2.4:1, and high SA *S* decreased with half-lives of 1.9 and 21 min with a ratio of 1.9:1. On average, the fraction of total plasma activity represented by [^{11}C]rolipram in high SA *R* experiments decreased to 51% at 6.5 min and to 21% at 12 min. Fraction of [^{11}C]rolipram in low SA *R* experiments decreased to 51% at 11 min and to 22% at 41 min. Fraction of [^{11}C]rolipram in high SA *S* experiments decreased to 51% at 11 min and 22% at 45 min. *R* and *S* enantiomers showed similar levels of protein binding, with f_1 values of 25% and 28%, respectively. Because of the similar plasma protein binding, it was appropriate to use V'_T instead of V_T to compare measurements among the three paradigms.

Nonlinear least squares analysis

Fig. 4 shows representative fitting by one- and unconstrained two-compartment models in high SA *R*, low SA *R*, and high SA *S* experiments. In other regions, differences of the fitting by these two models and goodness-of-fit were similar. In all regions of all experiments in the three paradigms, *F* tests indicated that the two-compartment model gave significantly better fitting ($P < 0.025$ in all regions, $P < 0.0005$ in 70 of 80 comparisons).

Table 2 shows rate constants in high SA *R* experiments obtained by the one-compartment model. Results in parietal cortex are shown as representative of cerebral cortices. Each rate constant (K_1 and k'_2) and the distribution volume, V'_T, were well identified. K_1 and V'_T were particularly well identified with COV below 5%. Mean intersubject variability of V'_T in eight regions expressed by SD/mean was 25%. Consistent with the in vivo distribution of rolipram binding shown in Fig. 2, V'_T in hypothalamus and midbrain were smaller than that in other regions. Although thalamus showed rapid uptake (i.e., high K_1 values), washout (i.e., k'_2) was also high, and hence the distribution volume, V'_T ($=K_1/k'_2$), was not particularly high. Low SA *R* experiments showed average K_1, k'_2, and V'_T values of 0.43 mL cm^{-3} min^{-1}, 0.26 min^{-1}, and 1.75 mL cm^{-3}, respectively, in the studied regions. COV values of these experiments were greater than those of high SA *S* experiments with average values of 9.0, 12, and 5.8% for K_1, k'_2, and V'_T, respectively. MANOVA indicated that low SA *R* experiments gave greater COV of V'_T than high SA *R* ($P = 0.038$) and high SA *S* experiments ($P = 0.005$). Goodness-of-fit of low SA *R* experiments (MSC = 1.4) was worse than that of high SA *R* ($P = 0.022$) but not that of high SA *S* experiments. High SA *S* experiments showed average K_1, k'_2, and V'_T values of 0.73, 0.25, and 2.96, respectively, in the studied regions. COV of these experiments was similar to those of high SA *R* experiments with average values of 4.6, 6.6 and 3.1 for K_1, k'_2, and V'_T, respectively. Goodness-of-fit of high SA *S* experiments was also similar to that of high SA *R* experiments showing a mean MSC value of 2.8.

Table 3 shows results of the two-compartment model in high SA *R* experiments. Although *F* tests indicated that the two-compartment model gave significantly better fitting in all regions of all experiments in the three paradigms than the one-compartment model, the former did not identify rate constants as well as the latter as indicated by greater COVs ($P < 0.0005$ for V'_T). Although COVs of K_1 were low and similar to those by the one-compartment model, other rate constants, particularly k_3 and k_4 showed large COV values ranging from 18 to 37%. Despite poor identifiability of each rate constant by the two-compartment model, COVs of V'_T stayed at reasonably low levels below 10% and were

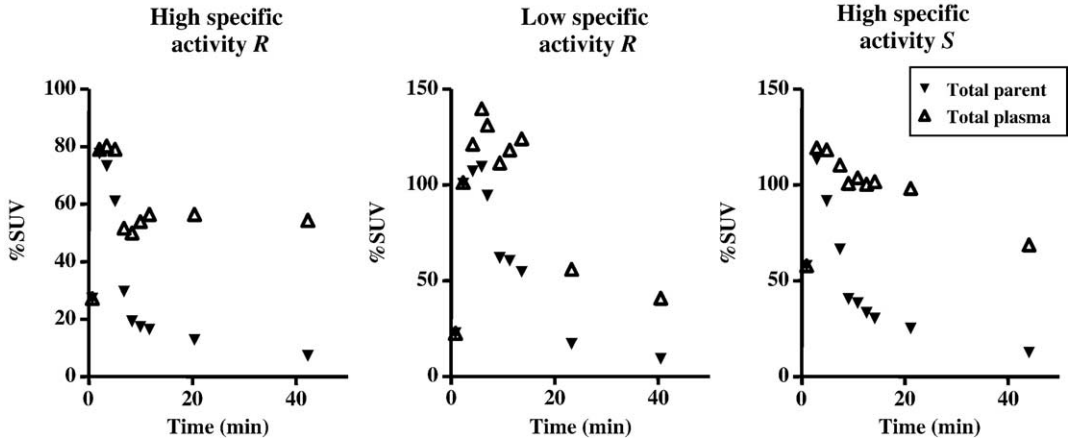

Fig. 3. [^{11}C]Rolipram and total plasma activities in the three PET experiments shown in Fig. 1. In all experiments, [^{11}C]rolipram was cleared quickly from plasma decreasing to less than half of the peak within 10 min.

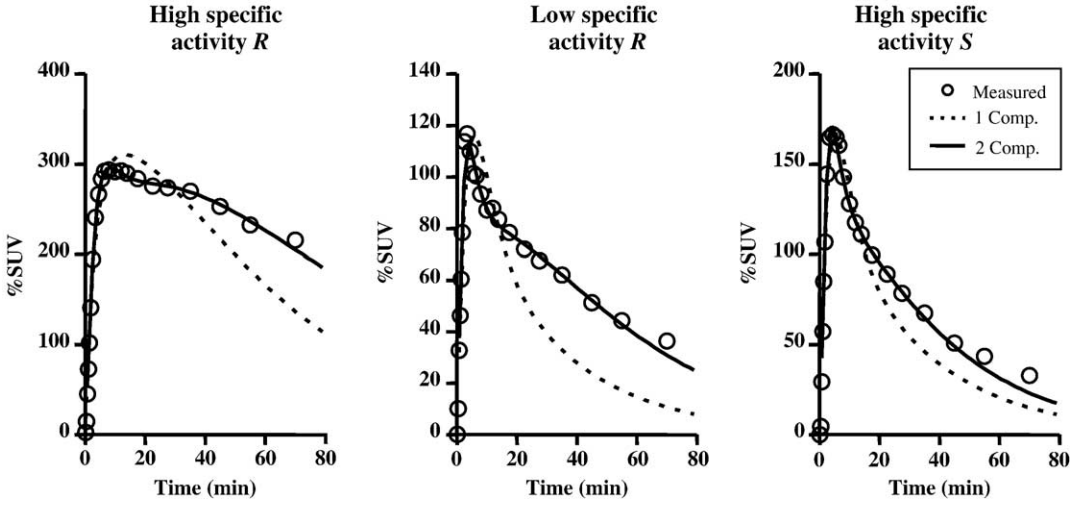

Fig. 4. Nonlinear least squares fitting by one- and two-compartment models for parietal cortex data in the three experiments shown in Figs. 1 and 3. In all experiments, F tests indicated significantly better fitting by the two-compartment model.

approximately twice of those by the one-compartment model. The two-compartment model achieved reasonably good identifiability of V_T' ($=K_1k_3/k_2k_4$) despite poor identifiability of some individual parameters because of correlation among parameters. For example, k_3 and k_4 correlated well with $r = 0.72$ ($P < 0.0005$). As indicated by the poor fitting in Fig. 4, the one-compartment model showed smaller V_T' values than the two-compartment model in all regions in all high SA R experiments ($P < 0.0005$). The average differences in eight regions in six high SA R experiments were 19–31%. Average intersubject variability of V_T' in the studied regions, expressed by SD/mean, was 23%, which was similar to that of the one-compartment model. Therefore, although the one-compartment model showed excellent identifiability of parameters, it underestimated V_T' because of the poor fitting, and the two-compartment model gave more accurate V_T'.

Low SA R experiments showed average K_1, k_2, k_3, k_4, and V_T' values of 2.0 mL cm^{-3} min^{-1}, 1.8 min^{-1}, 0.050 min^{-1}, 0.022 min^{-1}, and 3.2 mL cm^{-3}, respectively, in the studied regions. Similar to the results by the one-compartment model, COV values of these experiments were greater than those of high SA R experiments with average values of 13, 16, 21, 51, and 24% for K_1, k_2, k_3, k_4, and V_B', respectively (for V_B', $p = 0.027$ compared to high SA R and $P = 0.022$ compared to high SA S experiments). Goodness-of-fit of low SA R experiments was worse than that of high SA R experiments showing a mean MSC value of 3.3 ($P = 0.001$). High SA S experiments showed average K_1, k_2, k_3, k_4, and V_T' values of 1.8, 1.1, 0.092, 0.090, and 3.4, respectively, in the studied regions. COV of these studies was similar to those of high SA R experiments with average values of 9.2, 14, 23, 21, and 4.5 for K_1, k_2, k_3, k_4, and V_B', respectively. Goodness-of-fit of high SA S experiments was also similar to that of high SA R experiments showing a mean MSC value of 4.1.

High SA R experiments showed much greater V_T' values (16.4–29.2 mL cm^{-3}) than low SA R (2.9–3.5) and high SA S (3.1–3.7) experiments (Fig. 5). Although low SA R and high SA S experiments showed fairly uniform distribution of V_T' among brain regions, high SA R experiments showed substantial differences among brain regions. Average V_T' of all regions in low SA R and high SA S experiments was 14% of that of high SA R experiments.

Discussion

The present study using rats and a small animal PET scanner has confirmed findings in previous non-human primate and human studies that (R)-[^{11}C]rolipram has favorable characteristics as a brain imaging agent. In the present study, (R)-[^{11}C]rolipram showed good initial brain uptake of approximately 300 SUV% and the washout was measurable within 2–3 half-lives of carbon-11 (Figs. 1 and 4). Quantification in the present study also showed high levels of specific binding in high SA R experiments. As described below, because there is no measurable binding site free region, and input function may be different in each experiment, calculation of distribution volume with arterial input function is required for accurate measurement. Because of the small body size of rats, it was challenging to perform quantification with a metabolite-corrected arterial input function. Nevertheless, in the present study, an unconstrained two-compartment model showed

Table 2
Results of high SA R experiments by one-compartment model

Region	K_1 (mL cm^{-3} min^{-1})	k_2' (min^{-1})	V_T' (mL cm^{-3})	*MSC*
Caudate putamen	1.15 ± 0.28 (2.5 ± 0.7)	0.051 ± 0.014 (5.7 ± 0.9)	23.3 ± 5.7 (3.9 ± 0.6)	3.3 ± 0.6
Thalamus	1.14 ± 0.25 (2.8 ± 1.0)	0.065 ± 0.016 (5.9 ± 1.3)	18.2 ± 4.5 (3.8 ± 0.6)	3.1 ± 0.7
Hypothalamus	0.95 ± 0.22 (3.4 ± 1.3)	0.076 ± 0.021 (6.7 ± 1.7)	13.1 ± 3.4 (4.2 ± 0.8)	2.7 ± 0.7
Parietal cortex	0.82 ± 0.18 (2.4 ± 0.8)	0.045 ± 0.010 (5.8 ± 1.1)	18.8 ± 4.6 (4.1 ± 0.7)	3.3 ± 0.6
Midbrain	1.21 ± 0.30 (4.0 ± 1.1)	0.094 ± 0.025 (7.3 ± 1.3)	13.3 ± 3.2 (4.4 ± 0.6)	2.4 ± 0.5

Numbers in parentheses indicate identifiably of rate constants expressed as %COV.
MSC: Model Selection Criterion.

Table 3
Results of high SA *R* experiments by two-compartment model

Regions	K_1 (mL cm^{-3} min^{-1})	k_2 (min^{-1})	k_3 (min^{-1})	k_4 (min^{-1})	V'_T (mL cm^{-3})	*MSC*
Caudate putamen	1.31 ± 0.30 (2.8 ± 1.4)	0.13 ± 0.08 (14 ± 11)	0.069 ± 0.059 (37 ± 22)	0.039 ± 0.015 (35 ± 22)	29.2 ± 6.8 (9.3 ± 4.3)	4.9 ± 0.4
Thalamus	1.39 ± 0.33 (2.4 ± 0.3)	0.17 ± 0.10 (10 ± 4)	0.072 ± 0.032 (23 ± 10)	0.045 ± 0.017 (24 ± 19)	23.1 ± 5.1 (7.9 ± 9.1)	5.1 ± 0.5
Hypothalamus	1.25 ± 0.28 (4.5 ± 1.5)	0.25 ± 0.11 (15 ± 7)	0.116 ± 0.058 (25 ± 8)	0.055 ± 0.025 (23 ± 20)	16.4 ± 3.3 (8.8 ± 10.1)	4.2 ± 0.4
Parietal cortex	0.96 ± 0.24 (2.2 ± 0.9)	0.12 ± 0.05 (10 ± 4)	0.065 ± 0.039 (25 ± 14)	0.033 ± 0.012 (29 ± 20)	25.2 ± 5.4 (9.8 ± 6.6)	5.3 ± 0.5
Midbrain	1.62 ± 0.43 (3.3 ± 0.7)	0.27 ± 0.09 (9 ± 3)	0.086 ± 0.039 (18 ± 7)	0.045 ± 0.018 (20 ± 15)	17.8 ± 3.6 (7.6 ± 7.1)	4.5 ± 0.5

Numbers in parentheses indicate identifiably of constants expressed as %COV.
MSC: Model Selection Criterion.

reasonably good identifiability of V'_T with an average %COV smaller than 10% and small intersubject variability (SD/mean) of 23% (Table 3 and Fig. 5). Low SA *R* (average V'_T = 3.2 mL cm^{-3}) and high SA *S* (average V'_T = 3.4) experiments showed similar and fairly uniform distribution of V'_T indicating that V'_T by these two paradigms represented nondisplaceable (free + non-specific binding) distribution volumes. By comparing V'_T obtained in high SA *R* and average V'_T in low SA *R* and high SA *S* experiments, majority (82–88%, average = 86%) of V'_T in high SA *R* studies reflected specific binding (Fig. 5).

Higher injected activities are required to obtain image data with better statistics, especially in small volumes of interest. However, greater injection activities increase the mass dose and the receptor occupancy by the radioligand. Please note that we have used classical receptor binding theory to analyze the reversible binding of rolipram to the enzyme PDE4. Therefore, binding site occupancy is often a problem in small animal PET studies, and a simple method was proposed to estimate in vivo binding site occupancy using the dose required to reduce the maximal effects or binding by one-half (ED_{50} or IC_{50}) (Hume et al., 1998). Before starting the study, we estimated required specific activity using the formula proposed by Hume et al. Based on literature reporting in vivo effects of rolipram (Griebel et al., 1991; Heaslip and Evans, 1995; Lourenco et al., 2001; O'Donnell, 1993; Schultz and Schmidt, 1986) to keep binding site occupancy to 5% or less by injecting 110 MBq (*R*)-[^{11}C]rolipram to a 300-g rat, specific activity must be 38 GBq/μmol or greater. In all of the high SA *R* experiments, specific activity was greater than 38 GBq/μmol.

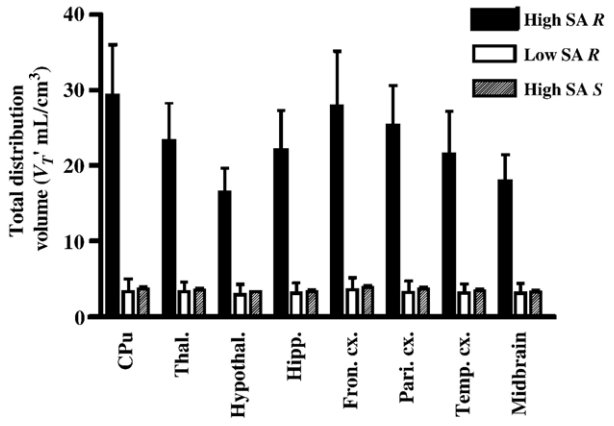

Fig. 5. Total distribution volume (V'_T) in high SA *R*, low SA *R*, and high SA *R* experiments obtained by the two-compartment model. High SA *R* experiments showed much greater V'_T than the other two paradigms. Low SA *R* and high SA *S* experiments showed fairly uniform regional distribution.

Further, there was not even a trend of positive correlation between specific activity and V'_T in any brain region in high SA *R* experiments (largest r = 0.37, P = 0.47). Therefore, the high SA *R* experiments were performed under true tracer conditions, with the radioligand having negligible binding site occupancy. Because we have confirmed that the majority of V'_T of (*R*)-[^{11}C]rolipram was specific binding, we did not perform a binding inhibition study by changing dose of non-radiolabeled (*R*)-rolipram as performed in porcine (Parker et al., 2005) to measure binding site occupancy. A reservation on in vivo binding inhibition assays is possible biological effects of non-radiolabeled (*R*)-rolipram and changes of rate constants during experiments as discussed below and in the study in porcine (Parker et al., 2005).

PET quantification of neurotransmission systems is significantly simplified if there is a brain region with negligible density of the binding site (i.e., reference tissue). In such cases, B_{max}'/K_d is estimated using reference-tissue instead of arterial input function. However, rat in vitro autoradiography studies did not identify a binding site-free region of adequate size to be visible in PET images (Kaulen et al., 1989; Perez-Torres et al., 2000). Among the brain regions studied, most areas in midbrain showed low binding densities with in vitro autoradiography (Kaulen et al., 1989). However, V'_T of midbrain measured in our PET high SA *R* experiments was as much as 5.5 times greater than that of low SA *R* and high SA *S* experiments. Thus, the limited resolution of in vivo PET cannot visualize a binding site poor region and measurement of arterial input function is required for quantitation of PDE4.

Fig. 5 shows heterogeneity of V'_T obtained in high SA *R* experiments. Because rat in vitro autoradiography studies (Kaulen et al., 1989; Perez-Torres et al., 2000) divided brain areas to small regions, and one of these studies reported only semiquantitative results, it is difficult to compare the distribution of V'_T obtained by PET and the binding distribution by in vitro autoradiography. Nevertheless, the distribution obtained by these two different techniques roughly matched with high binding in frontal cortex, low binding in hypothalamus and midbrain, and medium levels in other regions. However, the high V'_T in caudate putamen obtained by PET does not seem to match well with results by the autoradiographic studies. As described above, in vivo binding of rolipram might reflect phosphorylation of PDE4, and different phosphorylation states between in vivo and in vitro conditions might have caused this difference.

Significantly poorer identifiability of V'_T in low SA *R* might have been caused by biological changes of PDE4 caused by the high dose of rolipram, and rate constants might have not been constant during experiments. For example, a study has indicated that inhibitors of PDE4 cause conformational changes and cause redistribution in the cell (Terry et al., 2003). Such changes would significantly alter access and binding of rolipram to PDE4 and its

dissociation. To take into account possible differences of input function among experiments, particularly among those with high SA *R*, low SA *R*, and low SA *S*, arterial input function was measured in every experiment. Although a small number of experiments were performed, there appeared to be differences in input function among high SA *R*, low SA *R*, and high SA *S* experiments. A speculation is that the high mass dose in low SA *R* experiments induced changes in enzymes that metabolized rolipram. Cautions should be paid if specific binding distribution volume, V_S, is estimated by subtracting brain activity of an *S* experiments from that of a high SA *R* (Tsukada et al., 2001) because input function may be different between these two studies. In rat, because majority (~86%) of V'_T was specific binding, specific binding of (*R*)-rolipram is estimated well by measuring V'_T of (*R*)-[^{11}C]rolipram by obtaining arterial input function. Both in one- and two-compartment models, although K_1 values were well identified, the numbers are much greater than those of many PET ligands obtained in humans. It should be noted that rats have much greater cerebral blood flow than humans (Grome and Harper, 1983), and considering the lipophilicity and molecular weight of rolipram, K_1 values obtained in this study are reasonable.

In summary, binding of (*R*)-[^{11}C]rolipram was accurately measured by applying an unconstrained two-tissue compartment model with arterial input function. The brain uptake of (*R*)-[^{11}C]rolipram was saturable, since the low SA *R* experiments showed blockade with the co-injection of nonradioactive carrier. Nonspecific uptake was relatively low, as determined from low SA *R* and high SA *S* experiments. Because the majority (~86%) of V'_T of (*R*)-[^{11}C]rolipram was specific binding, V'_T reflected specific binding. The quantification established in the present study can now be applied to study rodent models where changes in the cAMP system are expected.

Acknowledgments

The authors thank C. Burger, PhD, P. Rudnicki, PhD, K. Mikolajczyk, PhD, M. Grodzki, PhD, and M. Szabatin, PhD for providing PMOD 2.55. The authors also thank P. F. Morrison, PhD, L. Chang, PhD, and S. I. Rapoport, MD for assisting ex vivo autoradiography experiments and H. Toyama, MD, PhD, for setting up laboratory equipments for PET studies.

References

Akaike, H., 1974. A new look at the statistical model identification. IEEE Trans. Autom. Control AC19, 716–723.

Bevington, P.R., Robinson, D.K., 2003. Data Reduction and Error Analysis for the Physical Sciences. McGraw-Hill, New York.

Burger, C., Mikolajczyk, K., Grodzki, M., Rudnicki, P., Szabatin, M., Buck, A., 1998. JAVA tools quantitative post-processing of brain PET data. J. Nucl. Med. 39, 277P.

Carson, R.E., 1986. Parameter estimation in positron emission tomography. In: Phelps, M.E., Mazziotta, J.C., Schelbert, H.R. (Eds.), Positron Emission Tomography and Autoradiography: Principles and Applications for the Brain and Heart. Raven Press, New York, pp. 347–390.

Conti, M., Nemoz, G., Sette, C., Vicini, E., 1995. Recent progress in understanding the hormonal regulation of phosphodiesterases. Endocr. Rev. 16, 370–389.

DaSilva, J.N., Lourenco, C.M., Meyer, J.H., Hussey, D., Potter, W.Z., Houle, S., 2002. Imaging cAMP-specific phosphodiesterase-4 in human brain with *R*-[^{11}C]rolipram and positron emission tomography. Eur. J. Nucl. Med. Mol. Imaging 29, 1680–1683.

Duman, R.S., Heninger, G.R., Nestler, E.J., 1997. A molecular and cellular theory of depression. Arch. Gen. Psychiatry 54, 597–606.

Fleischhacker, W.W., Hinterhuber, H., Bauer, H., Pflug, B., Berner, P., Simhandl, C., Wolf, R., Gerlach, W., Jaklitsch, H., Sastre-y-Hernandez, M., et al., 1992. A multicenter double-blind study of three different doses of the new cAMP-phosphodiesterase inhibitor rolipram in patients with major depressive disorder. Neuropsychobiology 26, 59–64.

Fujita, M., Seibyl, J.P., Verhoeff, N.P.L.G., Ichise, M., Baldwin, R.M., Zoghbi, S.S., Burger, C., Staley, J.K., Rajeevan, N., Charney, D.S., Innis, R.B., 1999. Kinetic and equilibrium analyses of [^{123}I]epidepride binding to striatal and extrastriatal dopamine D_2 receptors. Synapse 34, 290–304.

Gandelman, M.S., Baldwin, R.M., Zoghbi, S.S., Zea-Ponce, Y., Innis, R.B., 1994. Evaluation of ultrafiltration for the free fraction determination of single photon emission computed tomography (SPECT) tracers: β-CIT, IBF, and iomazenil. J. Pharm. Sci. 83, 1014–1019.

Griebel, G., Misslin, R., Vogel, E., Bourguignon, J.J., 1991. Behavioral effects of rolipram and structurally related compounds in mice: behavioral sedation of cAMP phosphodiesterase inhibitors. Pharmacol. Biochem. Behav. 39, 321–323.

Grome, J.J., Harper, A.M., 1983. The effects of serotonin on local cerebral blood flow. J. Cereb. Blood Flow Metab. 3, 71–77.

Hawkins, R.A., Phelps, M.E., Huang, S.-C., 1986. Effects of temporal sampling, glucose metabolic rates, and disruptions of the blood–brain barrier on the FDG model with and without a vascular compartment: studies in human brain tumors with PET. J. Cereb. Blood Flow Metab. 6, 170–183.

Heaslip, R.J., Evans, D.Y., 1995. Emetic, central nervous system, and pulmonary activities of rolipram in the dog. Eur. J. Pharmacol. 286, 281–290.

Hoffmann, R., Wilkinson, I.R., McCallum, J.F., Engels, P., Houslay, M.D., 1998. cAMP-specific phosphodiesterase HSPDE4D3 mutants which mimic activation and changes in rolipram inhibition triggered by protein kinase A phosphorylation of Ser-54: generation of a molecular model. Biochem. J. 333, 139–149.

Houslay, M.D., 2001. PDE4 cAMP-specific phosphodiesterases. Prog. Nucleic Acid Res. Mol. Biol. 69, 249–315.

Hume, S.P., Gunn, R.N., Jones, T., 1998. Pharmacological constraints associated with positron emission tomographic scanning of small laboratory animals. Eur. J. Nucl. Med. 25, 173–176.

Johnson, C.A., Seidel, J., Vaquero, J.J., Pascau, J., Desco, M., Green, M.V., 2002. Exact positioning for OSEM reconstructions on the ATLAS depth-of-interaction small animal scanner. Mol. Imaging Biol. 4, S22.

Kaulen, P., Bruning, G., Schneider, H.H., Sarter, M., Baumgarten, H.G., 1989. Autoradiographic mapping of a selective cyclic adenosine monophosphate phosphodiesterase in rat brain with the antidepressant [^{3}H]rolipram. Brain Res. 503, 229–245.

Laruelle, M., Baldwin, R.M., Rattner, Z., Al-Tikriti, M.S., Zea-Ponce, Y., Zoghbi, S.S., Charney, D.S., Price, J.C., Frost, J.J., Hoffer, P.B., Innis, R.B., 1994. SPECT quantification of [^{123}I]iomazenil binding to benzodiazepine receptors in nonhuman primates: I. Kinetic modeling of single bolus experiments. J. Cereb. Blood Flow Metab. 14, 439–452.

Liow, J., Seidel, J., Johnson, C.A., Toyama, H., Green, M.V., Innis, R.B., 2003. A single slice rebinning/2D exact positioning OSEM reconstruction for the NIH ATLAS small animal PET scanner. J. Nucl. Med. 44, 163P.

Lourenco, C.M., DaSilva, J.N., Warsh, J.J., Wilson, A.A., Houle, S., 1999. Imaging of cAMP-specific phosphodiesterase-IV: comparison of [^{11}C]rolipram and [^{11}C]Ro 20-1724 in rats. Synapse 31, 41–50.

Lourenco, C.M., Houle, S., Wilson, A.A., DaSilva, J.N., 2001. Characterization of R-[^{11}C]rolipram for PET imaging of phosphodieterase-4: in vivo binding, metabolism, and dosimetry studies in rats. Nucl. Med. Biol. 28, 347–358.

Matthews, J.C., Passchier, J., Wishart, M.O., Martarello, L., Comley, R.A.,

Parker, C.A., Knibb, S.T., Hopper, R.V., Brown, J., Gee, A.D., 2003. The characterisation of both the R and S enantiomers of [^{11}C]rolipram in man. J. Cereb. Blood Flow Metab. 23, 678.

Mizokawa, T., Kimura, K., Ikoma, Y., Hara, K., Oshino, N., Yamamoto, T., Ueki, S., Wachtel, H., 1988. The effect of a selective phosphodiesterase inhibitor, rolipram, on muricide in olfactory bulbectomized rats. Potential antidepressant activity of rolipram and other selective cyclic adenosine 3′,5′-monophosphate phosphodiesterase inhibitors. Jpn. J. Pharmacol. 48, 357–364.

Nestler, E.J., Aghajanian, G.K., 1997. Molecular and cellular basis of addiction. Science 278, 58–63.

O'Donnell, J.M., 1993. Antidepressant-like effects of rolipram and other inhibitors of cyclic adenosine monophosphate phosphodiesterase on behavior maintained by differential reinforcement of low response rate. J. Pharmacol. Exp. Ther. 264, 1168–1178.

O'Donnell, J.M., Zhang, H.T., 2004. Antidepressant effects of inhibitors of cAMP phosphodiesterase (PDE4). Trends Pharmacol. Sci. 25, 158–163.

Parker, C.A., Matthews, J.C., Gunn, R.N., Martarello, L., Cunningham, V.J., Dommett, D., Knibb, S.T., Bender, D., Jakobsen, S., Brown, J., Gee, A.D., 2005. Behaviour of [^{11}C]*R*(−)- and [^{11}C]*S*(+)-rolipram in vitro and in vivo, and their use as PET radiotracers for the quantificative assay of PDE4. Synapse 55, 270–279.

Perez-Torres, S., Miro, X., Palacios, J.M., Cortes, R., Puigdomenech, P., Mengod, G., 2000. Phosphodiesterase type 4 isozymes expression in human brain examined by in situ hybridization histochemistry and [^{3}H]rolipram binding autoradiography. Comparison with monkey and rat brain. J. Chem. Neuroanat. 20, 349–374.

Schneider, H.H., Schmiechen, R., Brezinski, M., Seidler, J., 1986. Stereospecific binding of the antidepressant rolipram to brain protein structures. Eur. J. Pharmacol. 127, 105–115.

Schultz, J.E., Schmidt, B.H., 1986. Rolipram, a stereospecific inhibitor of calmodulin-independent phosphodiesterase, causes beta-adrenoceptor subsensitivity in rat cerebral cortex. Naunyn-Schmiedeberg's Arch. Pharmacol. 333, 23–30.

Schweinhardt, P., Fransson, P., Olson, L., Spenger, C., Andersson, J.L., 2003. A template for spatial normalisation of MR images of the rat brain. J. Neurosci. Methods 129, 105–113.

Seidel, J., Vaquero, J.J., Green, M.V., 2003. Resolution uniformity and sensitivity of the NIH ATLAS small animal PET scanner: comparison to simulated LSO scanners without depth-of-interaction capability. IEEE Trans. Nucl. Sci. 50, 1347–1350.

Takahashi, M., Terwilliger, R., Lane, C., Mezes, P.S., Conti, M., Duman, R.S., 1999. Chronic antidepressant administration increases the expression of cAMP-specific phosphodiesterase 4A and 4B isoforms. J. Neurosci. 19, 610–618.

Terry, R., Cheung, Y.F., Praestegaard, M., Baillie, G.S., Huston, E., Gall, I., Adams, D.R., Houslay, M.D., 2003. Occupancy of the catalytic site of the PDE4A4 cyclic AMP phosphodiesterase by rolipram triggers the dynamic redistribution of this specific isoform in living cells through a cyclic AMP independent process. Cell Signalling 15, 955–971.

Tsukada, H., Harada, N., Ohba, H., Nishiyama, S., Kakiuchi, T., 2001. Facilitation of dopaminergic neural transmission does not affect [^{11}C]SCH23390 binding to the striatal D_1 dopamine receptors, but the facilitation enhances phosphodiesterase type-IV activity through D1 receptors: PET studies in the conscious monkey brain. Synapse 42, 258–265.

Wachtel, H., 1983. Potential antidepressant activity of rolipram and other selective cyclic adenosine 3′,5′-monophosphate phosphodiesterase inhibitors. Neuropharmacology 22, 267–272.

Waterhouse, R.N., 2003. Determination of lipophilicity and its use as a predictor of blood–brain barrier penetration of molecular imaging agents. Mol. Imaging Biol. 5, 376–389.

Ye, Y., Conti, M., Houslay, M.D., Farooqui, S.M., Chen, M., O'Donnell, J.M., 1997. Noradrenergic activity differentially regulates the expression of rolipram-sensitive, high-affinity cyclic AMP phosphodiesterase (PDE4) in rat brain. J. Neurochem. 69, 2397–2404.

Zhao, Y., Zhang, H.T., O'Donnell, J.M., 2003. Antidepressant-induced increase in high-affinity rolipram binding sites in rat brain: dependence on noradrenergic and serotonergic function. J. Pharmacol. Exp. Ther. 307, 246–253.